Hittite Journal of Science and Engineering, 2022, 9 (3) 205–211
ISSN NUMBER: 2148–4171
DOI: 10.17350/HJSE19030000272

Path Tracking and Connection Mechanism of a Reconfigurable, Foldable, Legged, and Miniature Robot

Mustafa Ugur **Muhammed Uygun** **Alihan Bakir** **Onur Ozcan**
Bilkent University, Department of Mechanical Engineering, Ankara, Turkey

ABSTRACT

This work introduces the reconfigurable, foldable, legged, and miniature robot (REMIRO), a palm-size modular robot with compliant c-shaped legs. The robot's body modules are made by folding acetate sheets. The legs connected to these modules are made of Polydimethylsiloxane (PDMS) using molding. The backbone modules are made of Thermoplastic polyurethane (TPU) using 3D printing. In this study, we propose a path tracking algorithm for our robot that enables our modules to move from a random initial location to the pose required to lock with another module. We also design and manufacture backbones with embedded permanent magnets to allow connection between modules. We also present a kinematic model of our robot utilizing c-shaped leg kinematics, predicting the forward differential kinematics of the robot, which is then used to test the path tracking algorithm. Our experiments show that the proposed path tracking algorithm moves our robot to the desired location with an average positioning error of 5mm and an average orientation error of 22°, which are small enough to permit docking between modules.

Keywords:
Cellular and modular robots; Legged robots; Soft robot materials and design.

Article History:
Received: 2022/07/18
Accepted: 2022/08/31
Online: 2022/09/28

***Correspondence to**: Onur ÖZCAN,*
E-mail: onurozcan@bilkent.edu.tr;
Phone: +90 312 290 2893;
Fax: +90 312 266 4126.

INTRODUCTION

Over the last decade, several miniature robots have been proposed to be used for investigation operations in narrow spaces [1], [2]. These robots became popular because of their low cost, rapid prototyping, and high maneuverability [3], [4], [5]. With all of these capabilities, many different miniature robots have been designed to serve different duties with their interesting mechanical designs. Because of the lightweight nature of the miniature scale, researchers designed miniature jumping robots that can jump 27 times higher than their own height [6]. Some researchers also proposed controllers for their stance phase [7]. Several research groups also combined jumping and running and manufactured palm-size robots that can both run and jump [8], [9].

However, these miniature robots suffer from locomotion issues while moving in confined spaces such as collapsed buildings after natural disasters or closed areas like inside metal pipes. To tackle these problems, researchers proposed c-shaped legged robots. RHex is one of the first robots developed as c-shaped legged robots [10]. With the help of a c-shaped structure, the legs have compliance, and this helps the robot to have better locomotion over different terrains. But many of the c-shaped legged robots are on a bigger scale, and this makes them immobile in small, confined spaces.

To overcome these locomotion issues, reconfigurable miniature robots have been proposed by researchers [11]. Reconfigurable robots get together to complete a specific task, such as climbing an obstacle [12] or moving an object [13]. Then, when the task is completed, they separate from each other, and they can continue their independent tasks. The main motivation behind these robots comes from biology.

In nature, animals collaborate with each other to complete complex tasks more easily. An example of this collaboration can be given as the army ants. They build complicated structures to make some tasks possible for the whole group of ants while one ant cannot complete. For instance, they construct bridges over different places they want to fill, and they build those structures to speed up the movements of the whole colony from one place to another [14].

Social insects like ants, bees, or termites communicate with each other for different reasons. They might want to complete a task, they might be telling where

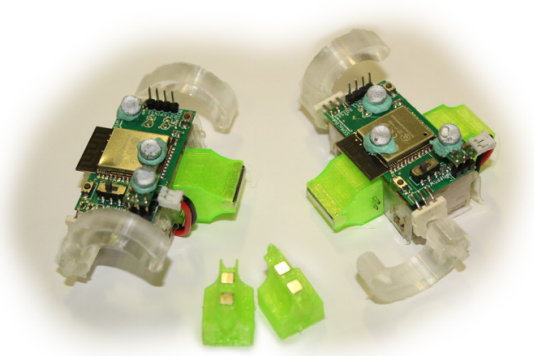

Figure 1. Two REMIRO modules with two different backbones. Three markers are attached to each module to track the positions of modules under the motion tracking system.

food is, or they may tell each other the state of the enemy. Those social insects can achieve this communication in different ways, e.g., using pheromones (scent), touch, body language, sound, and trophallaxis, which means sharing food [15]. At the end of the communication, insects can get various information, e.g., where to go for the food or where the enemy is. In a case, such as building a bridge, an ant first learns where to go for this task, then moves to that place and touches other ants. Finally, it determines how to dock with other ants.

Getting the inspiration from the collaboration between the army ants, we present a new reconfigurable, foldable, legged, and miniature robot (REMIRO). Shown in Fig. 1, REMIRO has foldable body modules, c-shaped compliant legs, and soft backbones. Modules of the robot have the capability to track a path with our proposed path-tracking algorithm and dock with each other successfully. The contributions of this work are the design of a new reconfigurable and miniature robot, a path tracking algorithm to move the modules, a backbone design to connect the modules, and the experimental results showing the locomotion behaviors of the modules.

MATERIAL AND METHODS

Our previous work [16], presents a soft, modular, legged robot with c-shaped legs (C-SMoLBot). It has a rigid body, compliant (soft) legs, and its backbones can be either rigid or soft depending on the design choice. Its modules are made of acetate sheets by folding, the backbones which connects these modules, and the compliant legs are made of PDMS using 3D printed molds. Each module has its own controller, and they communicate with each other via wired I^2C connection. Before the operation, the modules must be connected with metal pins to each other manually and communication cables around the modules have to be soldered. In other words, this robot, albeit modular, lacks the reconfigurability desired.

In our new robot, we aim to change our existing modular robot into a reconfigurable robot so that our modules can work on their own around the field and also can dock with each other when needed. For example, they can conduct surveillance missions around large environments and when they come across a big obstacle, they can dock and climb it, then undock and continue their own tasks.

To enable this reconfigurability, we propose a new robot design with c-shaped legs with a new controller board that can communicate wirelessly. In our new design, our robots can track a path under the motion tracking system and dock with each other with the help of our newly designed backbones. This section talks about the design and manufacturing of the robot, and backbones, gives an overview about the forward and inverse kinematics of the c-shaped legs, and mentions the proposed path tracking algorithm.

Design and Manufacturing of the Robot

REMIRO is an origami-inspired untethered robot that is made by folding an acetate sheet, as can be seen from the CAD drawings of a module shown in Fig. 2. It has two c-shaped soft legs, two dc motors, a Li-Po battery, and a control board. A single module weighs 30.3 grams and has the dimensions of 44.5mm x 24.2mm x 25mm without its legs.

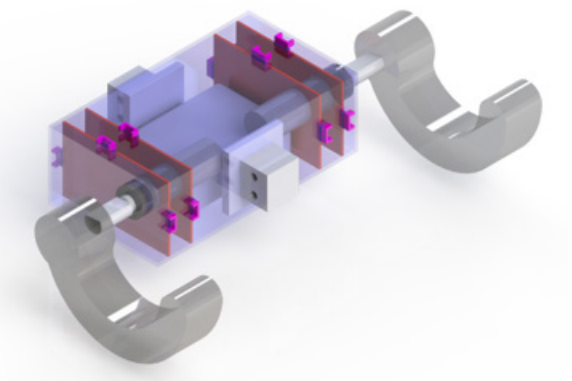

Figure 2. CAD drawing of one module of REMIRO.

As the first step of manufacturing, we laser cut previously designed 2D patterns. Then, we put the required 3D printed parts like motor holders, locks for connecting backbones, etc. Then, we put motors inside the holders, locks to the required places and conclude the folding process. After that, we solder the control board with rotary sensors, and this soldering holds the legs and the robot body together.

In the manufacturing of the c-shaped soft legs, we use Polydimethylsiloxane (PDMS) as the material with its curing agent. After mixing the PDMS and its curing agent, we put the mixture into a vacuum to get rid of the bubbles inside the mixture. Then, we fabricate a camshaft that connects

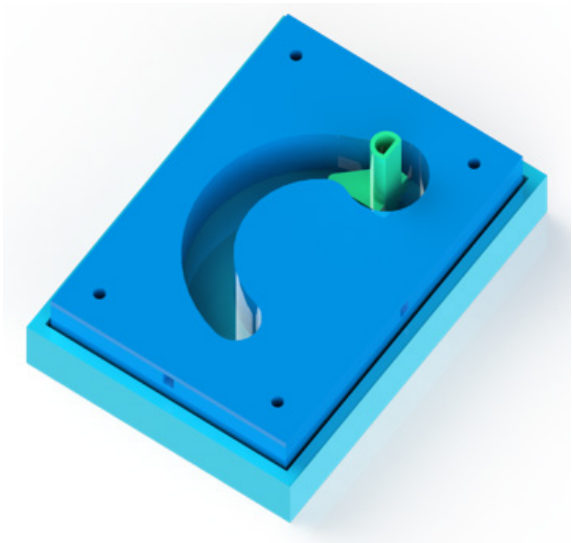

Figure 3. The CAD drawing of the mold for manufacturing the c-shaped leg. The light blue part is the bottom part of the mold, and the dark blue is the top part. The yellow part is the camshaft.

the leg with the motor with 3D printing. Finally, we put this camshaft inside its slot in the mold as shown in Fig. 3, pour the PDMS mixture inside the mold, and cure it for three hours in the oven at 60°C. We produce the molds with 3D printing as top and bottom parts. This separation eases the removal process.

As the last mechanical part of the robot, we manufacture backbones. Each module has two half backbones, one half in the front and one half in the rear and we produce them from Thermoplastic polyurethane (TPU) using 3D printing. Using TPU as the material provides compliance to the backbones. Backbones have two different variations that work as a locking mechanism. Indentation and protrusion places in the backbones for locking can be seen in Fig. 4 on each backbone. Also, by changing the thickness of these parts, the stiffness of the backbone can be controlled. Docking happens with the help of four permanent Neodymium magnets. These magnets have the size of 3.5mm x 3.5mm x 1.5mm. Horizontal holes provide locations to put pins to connect backbones with modules.

Each module has its electronic control board. This board has one ESP32-WROOM-32 module that has Wi-Fi, Bluetooth, and a microcontroller (ESP32-D0WDQ6). Other than these, each REMIRO module has a motor driver to control two DC motors separately and a 150 mAh Li-Po battery with a 3.7V supply. With all these capabilities, a single module REMIRO can serve as a fully untethered robot. Two infinite turn potentiometers are used as encoders for the feedback control. Using these sensors, the phase between the two legs in a single module can be controlled.

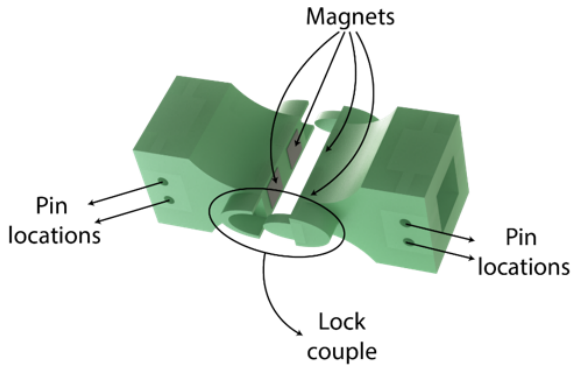

Figure 4. CAD drawings of a backbone couple. Four horizontal holes show the pin locations to lock with the module body, and grey squares are magnets that enables the connection. Lock couples on each side provide stiffness.

Forward and Inverse Differential Kinematics of the Robot

The single module of REMIRO is a differential drive robot that utilizes semi-circular c-shaped legs instead of fixed standard wheels. For a fixed standard wheel, the relation between the linear velocity ($\dot{x}$) and the angular velocity ($\dot{\varphi}$) of the wheel can be written as:

$$\dot{x} = r\dot{\varphi} \tag{1}$$

Whereas for the c-shaped legs, the relation between the linear velocity and the angular velocity is based on three modes of motion. These can be listed as rolling, overturning, and pure rotation [17]. We use following assumptions to determine the kinematic model c-shaped legs:

- No Slip: Relative velocity between the ground and the wheel contact point is zero.
- Rigid One-Dimension Semi-Circle Leg: C-shaped legs used for the REMIRO are compliant in order to enhance mobility. The position of the robot is naturally affected by the flexibility of the legs. However, for developing a model for the motion without dynamic calculations, rigidity is a core assumption.

Defining the mode of the motion (rolling, overturning, or pure rotation) according to the position of the camshaft, we can write the following equation to define the forward kinematics of the motion:

$$\begin{bmatrix} \dot{x} \\ \dot{y} \\ \dot{\theta} \end{bmatrix}_I = R(\theta)^{-1} \begin{bmatrix} \frac{r(\varphi_R)}{2} & \frac{r(\varphi_L)}{2} \\ 0 & 0 \\ \frac{r(\varphi_R)}{2l} & -\frac{r(\varphi_R)}{2l} \end{bmatrix} \begin{bmatrix} \dot{\varphi}_R \\ \dot{\varphi}_L \end{bmatrix} \tag{2}$$

In (2), φ_R and φ_L are the right and left leg's shaft angles, respectively. θ represents the orientation of the robot in a 2D space, and $R(\theta)$ represents the rotation matrix between the

inertial frame and the body frame, while l states the half of the length between the two legs. $\dot{x}$ and $\dot{\theta}$ represents the translational velocity *(v)* and rotational velocity *(ω)* in the inertial frame, respectively. $r(\varphi_R)$ and $r(\varphi_L)$ stands for the radius function that changes accoding to the three different motion modes. Lastly, subscript *I* shows that the vector is in inertial frame.

Similarly, we can express the inverse differential kinematics equations for our robot by using the effective radius instead of the constant radius value used for differential robots:

$$\begin{bmatrix}\dot{\varphi}_R\\ \dot{\varphi}_L\end{bmatrix}=\begin{bmatrix}\frac{1}{r(\varphi_R)} & 0 & \frac{1}{r(\varphi_L)}\\ \frac{1}{r(\varphi_L)} & 0 & -\frac{1}{r(\varphi_R)}\end{bmatrix}R(\theta)\begin{bmatrix}\dot{x}\\ \dot{y}\\ \dot{\theta}\end{bmatrix}_I \tag{3}$$

An important point to note about the inverse kinematic equations is that, in pure rotation mode of the motion, where $r(\varphi)=0$, the calculations for the rotation rate of the c-shaped legs approach to infinity. To solve this issue, a maximum frequency for the rotation is defined for this mode of the motion which is chosen as 2 Hz to prevent damaging the motor with overloading.

Because of the varying radius assumption, there is a difference between the simulations when we assume the robot as a differential-drive wheeled robot and the simulations when we use the varying radius assumption for the legs. Fig. 5 shows this difference. The blue line shows the robot running on 2Hz, during 5 seconds on trot gait where left and right legs have 180° phase differences. The red line shows the robot running on 2Hz, for 5 seconds, and in this case, we assume the robot as a differential-drive robot. As it can be seen from the straight line, when we assume it as a differential-drive, we cannot imply phase differences in the simulation. The difference between traveled distances is caused by the varying radius assumption. In this assumption robot does not move in the pure rotation mode of the motion and this causes robot to move less.

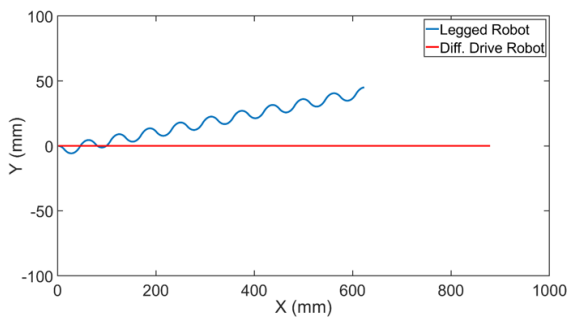

Figure 5. Forward kinematics simulations for the robot. The blue line shows the position of the robot for varying radius assumption, the red line shows the position of the robot for a differential-drive assumption.

Path Tracking of the Robot

As we mentioned above, animals use distinct ways to communicate and learn where to go for the task. Previously developed reconfigurable robots in the literature use different ways to find the goal position. For instance, researchers in [18] use LEDs and photoresistors mounted on their swarm robots. When a single module cannot accomplish a task, it turns on its LED, and the second robot moves toward the light source by measuring the light intensity at predetermined intervals. However, this method is only possible when there isn't a flooding external light source. Other researchers use RGB LEDs combined with a camera, proximity sensors, and an algorithm that makes use of a neural network that maps the data from the sensors to the motors [19]. In the robot named PolyBot, the system uses infrared proximity sensors to measure the distance between the modules [20]. Because there is limited space for electronic boards many miniature robots cannot use onboard positioning sensors. Some of them use overhead cameras [21], while others use external motion trackers to follow the position of their miniature reconfigurable robots [22], [23]. Because we need precise position data to control the motion of our modules, we use a motion tracking system (OptiTrack, Flex13) to receive the pose information of the modules. With the help of this information, we can control the modules to move toward each other.

Our modules with the ability to move each other can perform different swarm applications. For instance, one module of REMIRO has more mobility than a multi-module combination of the robot. One module can quickly move around confined spaces and easily maneuver, while a multi-module cannot fit or operate. However, when there is a need to climb an obstacle in the field, several modules of the REMIRO can dock to each other and climb the obstacle, then undock and continue their separate tasks. Because of these obligations, we use c-shaped legs that can improve the loco-

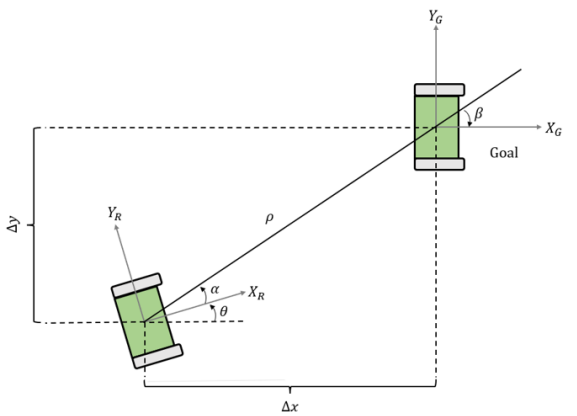

Figure 6. REMIRO module drawing, showing the path tracking of it from starting position (left and down) to the goal position (right and up).

motion performance on flat ground and obstacle climbing.

Because we have compliant c-shaped legs, there is always a gap between the mathematical motion models and the actual motion of the robot. This gap prevents us from implementing a path tracking algorithm without using feedback. In this work, we implement a feedback controller similar to the controller proposed in [24].

In Fig. 6, a REMIRO module can be seen that goes from a starting pose from the lower left to the goal pose in the upper right corner. In Fig. 6, ρ is the distance between the starting position and the goal position. α is the angle between the X_R and the ρ vector (goes from start to goal point). θ is the angle between the X_G and X_R. Finally, β is the angle between the ρ vector and X_G. The following equations give those values:

$$\rho = \sqrt{\Delta x^2 + \Delta y^2} \tag{4}$$

$$\alpha = -\theta + a\tan 2\left(\Delta y, \Delta x\right) \tag{5}$$

$$\beta = -\theta - \alpha \tag{6}$$

After calculating ρ,α, and β on each step, the feedback controller calculates the desired v (translational velocity) and ω (rotational velocity) as the controller output as shown in the following equations:

$$v = k_\rho \rho \tag{7}$$

$$w = k_\alpha \alpha + k_\beta \beta \tag{8}$$

To implement a controller that can work in every quadrant we need to check α value. If $\alpha \in \left(-\frac{\pi}{2}, \frac{\pi}{2}\right]$, we can use the translational velocity as it is shown in (7). But if $\alpha \in \left(-\pi, -\frac{\pi}{2}\right] \cup \left(\frac{\pi}{2}, -\pi\right]$, we must redefine the forward direction of the robot by setting $v = -v$. After calculating translational velocity ($\dot{x}$) and rotational velocity ($\dot{\theta}$), we calculate right and left leg velocities using eq. (3).

RESULTS AND DISCUSSION

As mentioned in the previous section, we use a motion tracking system to track the pose of the modules. This motion tracking system can provide 120 Hz pose data for two modules. As seen in Fig. 7, after we collect the pose data, the path tracking algorithm takes those poses as input and produces translational velocity and rotational velocity values as controller outputs. Then, we calculate right and left leg velocities. After calculating these frequency values, our control unit passes those values to the modules.

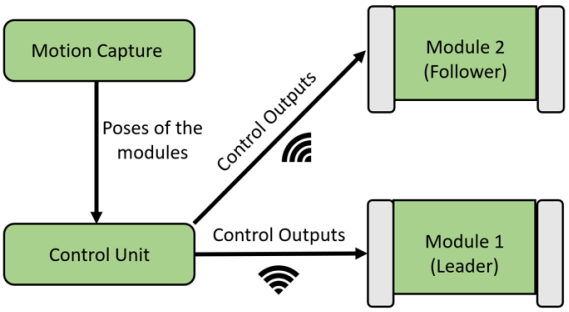

Figure 7. System architecture for communication.

In this work, we conduct experiments to see the success of the proposed forward kinematics model and the path tracking algorithm. Because we used compliant c-shaped legs to have better locomotion over different surfaces, we observe some differences between our simulation and experiment results. When our module runs on 2Hz with trot gait (180° phase difference between the legs), both simulations and experiments have a drift toward the +y direction as can be seen in Fig. 8. We also conduct the same experiment for the pronk gait (0° phase difference between the legs). Fig. 9 shows the results of the pronk gait simulations and experiments. In this case, our module maintains a straight line in its overall motion. In both experiments, we can see fluctuations. We can explain this motion characteristic with the use of compliant c-shaped legs, which brings a rocking

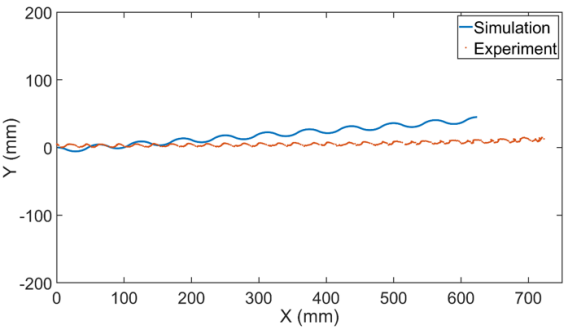

Figure 8. Forward kinematics simulations with an experiment for a module running on 2Hz with trot gait. The blue line represents the simulation result, while red markers represent the actual module running under the motion tracking system.

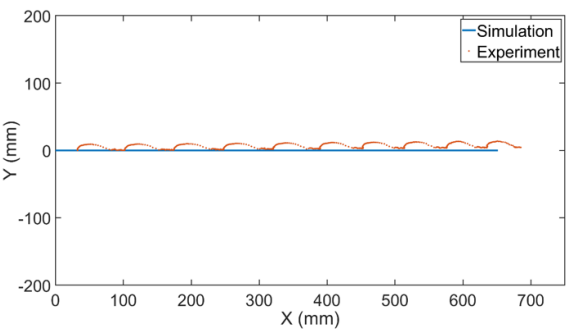

Figure 9. Forward kinematics simulations with an experiment for a module running on 2Hz with pronk gait. The blue line represents the simulation result, while red markers represent the actual module running under motion the tracking system.

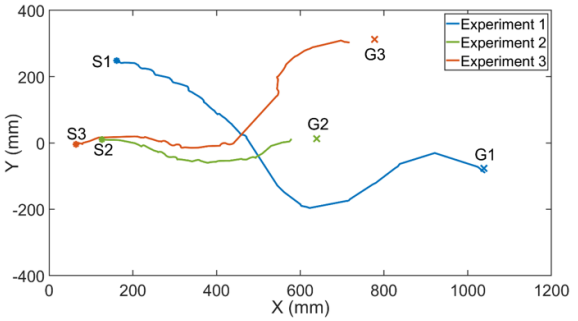

Figure 10. Path tracking experiments for one module. Each color represents a different trial. S1, S2, and S3 show the starting points, while G1, G2, and G3 show the goal points.

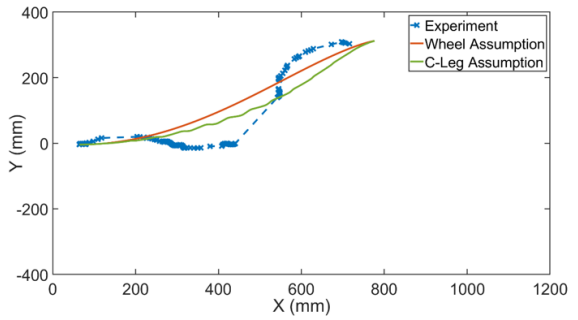

Figure 11. The path tracking experiment is shown with blue markers, the green line represents the simulation results for c-legged assumption, and the red line represents the simulation results for the wheeled assumption.

motion that cannot be fully captured with a 2D kinematic model.

We verify our path tracking algorithm with various experiments. Fig. 10 shows three different path tracking experiments. In these experiments, we place our modules to a starting pose, assign a goal pose, and investigate the motion from start to the goal position. Each color in the figure represents a different experiment, starting points are defined as S1, S2, and S3, while goal points are defined as G1, G2 and G3. In total we did five experiments, our modules were able to move to final poses with an average positioning error of 5 mm and an average orientation error of 22° . The main reason for these errors is again the compliant structure of the c-shaped legs and the kinematics differences between the c-shaped legs and standard wheels. In the experiments shown in Fig. 10, we assign a threshold value that stops the modules when they come close enough to the goal pose. Because of this threshold value our modules stops early sometimes and that is cause of the gaps between final points and the goal positions in the second and the third experiments. This threshold is set so that the modules do not bump into each other while docking, yet it is small enough that it does not affect docking performance negatively.

In wheeled differential-drive assumption, we cannot imply gaits. Also, we cannot imply three different mode motions that c-legged assumption has. Fig. 11 shows the simulation results for both wheel assumption (differential-drive), c-legged assumption (varying radius), and experiment results for the same starting point and goal point. Because of the soft c-shaped legs, there is a difference between simulations and the experiment. The difference between the simulations comes from the c-shaped leg assumption.

The proposed backbone design with magnets provides enough attraction force to keep the modules together during obstacle scaling and rough terrain locomotion. For instance, in our experiments, while a single-module-robot cannot climb a 15-mm-obstacle, when two modules are docked together, we observe that the robot can climb an obstacle with a height of 25 mm. Also, with the help of the proposed backbone design and the compliant c-shaped legs, our robot can move on terrain that is significantly rough compared to its size, such as a gravel-covered surface, as shown in Fig. 12.

CONCLUSION & FUTURE WORKS

In this work, we propose a path tracking algorithm for our reconfigurable, foldable, and miniature robot (REMIRO) and magnetic backbone design that enables the reconfigurable structure for our modules. Moreover, we apply c-legged kinematics to our robot's model to investigate the difference between the kinematics of our robot and the kinematics of a regular, wheeled differential drive robot. Our results indicate that our modules can move from one pose to another to dock with another module using the proposed path tracking algorithm. Also, our backbone design with permanent magnets can provide the required attraction force to keep the modules together while providing the needed soft structure in the backbones. This soft structure helps the robot to move around complex environments such as surfaces covered with gravel.

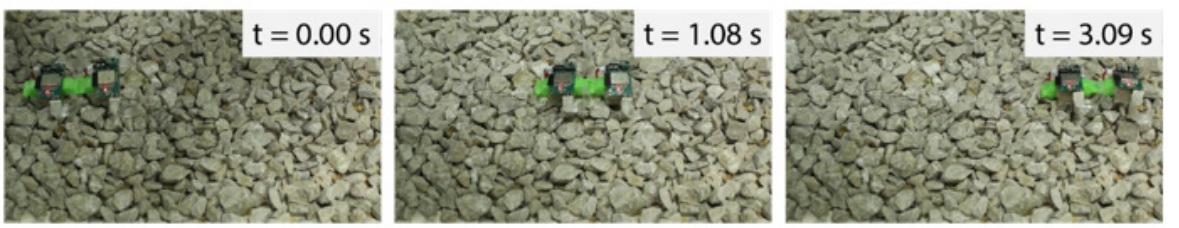

Figure 12. REMIRO with two modules moving on a surface covered with gravel.

In our future work, we are planning to conduct more experiments to further investigate the success rate of docking. Also, we are planning to implement an undocking procedure and a detection mechanism that can detect the docked modules. Finally, we are planning to conduct a comprehensive study on the locomotion characteristics of the reconfigurable robot.

CONFLICT OF INTEREST

Authors approve that to the best of their knowledge, there is not any conflict of interest or common interest with an institution/organization or a person that may affect the review process of the paper.

AUTHOR CONTRIBUTION

Mustafa Ugur: Conceptualization, Methodology, Software, Investigation, Formal Analysis, Writing- Original draft preparation.
Muhammed Uygun: Investigation, Formal Analysis
Alihan Bakir: Investigation, Formal Analysis
Onur Ozcan: Conceptualization, Supervision, Writing- Reviewing and Editing, Project Administration, Funding Acquisition.

REFERENCES

1. Mulgaonkar Y, Araki B, Koh JS, Guerrero-Bonilla L, Aukes DM, Makineni A, Tolley MT, Rus D, Wood RJ, Kumar V. The flying monkey: A mesoscale robot that can run, fly, and grasp. Paper presented at 2016 IEEE International Conference on Robotics and Automation (ICRA), Stockholm, Sweden, 16-21 May. IEEE, pp. 4672–4679, 2016.
2. Zarrouk D, Pullin A, Kohut N, Fearing RS. STAR, a sprawl tuned autonomous robot. Paper presented at 2013 IEEE International Conference on Robotics and Automation (ICRA), Karlsruhe, Germany, 6-10 May. IEEE, pp. 20-25, 2013.
3. Ozcan O, Baisch AT, Ithier D, Wood RJ. Powertrain selection for a biologically-inspired miniature quadruped robot. Paper presented at 2014 IEEE International Conference on Robotics and Automation (ICRA), Hong Kong, China, 31 May - 7 June, IEEE, pp. 2398–2405, 2014.
4. Rus D, Tolley MT. Design, fabrication and control of origami robots. Nature Reviews Materials 3 (2018) 101–112.
5. Mahkam N, Bakir A, Özcan O. Miniature Modular Legged Robot With Compliant Backbones. IEEE Robotics and Automation Letters 5 (2020) 3923–3930.
6. Kovac M, Fuchs M, Guignard A, Zufferey JC, Floreano D. A miniature 7g jumping robot. Paper presented at 2008 IEEE International Conference on Robotics and Automation (ICRA), Pasadena, CA, USA, 19-23 May, IEEE, pp. 373-378, 2008.
7. Yim JK, Singh BRP, Wang EK, Featherstone R, Fearing RS. Precision robotic leaping and landing using stance-phase balance. IEEE Robotics and Automation Letters 5 (2020) 3422- 3429.
8. Lambrecht BG, Horchler AD, Quinn RD. A small, insect-inspired robot that runs and jumps. Paper presented at 2005 IEEE International Conference on Robotics and Automation (ICRA), Barcelona, Spain, 18-22 April, IEEE, pp. 1240-1245, 2005.
9. Jung GP, Casarez CS, Lee J, Baek SM, Yim SJ, Chae SH, Fearing RS, Cho KJ. JumpRoACH: A trajectory-adjustable integrated jumping–crawling robot. IEEE/ASME Transactions on Mechatronics 24 (2019) 947-958.
10. Saranli U, Buehler M, Koditschek DE. RHex: A simple and highly mobile hexapod robot. The International Journal of Robotics Research 20 (2001) 616-631.
11. Brunete A, Ranganath A, Segovia S, de Frutos JP, Hernando M, Gambao E. Current trends in reconfigurable modular robots design. International Journal of Advanced Robotic Systems 14 (2017) 1–21.
12. Tosun T, Davey J, Liu C, Yim M. Design and characterization of the ep-face connector. Paper presented at 2016 IEEE/RSJ International Conference on Intelligent Robots and Systems (IROS), Daejeon, South Korea, 9-14 October, IEEE, pp. 45-51, 2016.
13. Spröwitz A, Moeckel R, Vespignani M, Bonardi S, Ijspeert AJ. Roombots: A hardware perspective on 3D self-reconfiguration and locomotion with a homogeneous modular robot. Robotics and Autonomous Systems 62 (2014) 1016-1033.
14. Reid CR, Lutz MJ, Powell S, Kao AB, Couzin ID, Garnier S. Army ants dynamically adjust living bridges in response to a cost–benefit trade-off. Proceedings of the National Academy of Sciences 112 (2015) 15113-15118.
15. LeBoeuf AC, Waridel P, Brent CS, Gonçalves AN, Menin L, Ortiz D, RibaGragnuz O, Koto A, Soares ZG, Privman E, Miska EA, Benton R, Keller L. Oral transfer of chemical cues, growth proteins and hormones in social insects. elife 5 (2016).
16. Mahkam N, Yılmaz TB, Özcan O, Smooth and Inclined Surface Locomotion and Obstacle Scaling of a C-Legged Miniature Modular Robot. Paper presented at 2021 IEEE 4th International Conference on Soft Robotics (RoboSoft), New Heaven, CT, USA, 12-16 April, IEEE, pp. 9-14, 2021. https://doi.org/10.1109/RoboSoft51838.2021.9479218
17. Vina A, Barrientos A. C-Legged Hexapod Robot Design Guidelines Based on Energy Analysis. Applied Sciences 11 (2021) 2513.
18. Aydin-Ozkan Y, Goldman D. Self-reconfigurable multilegged robot swarms collectively accomplish challenging terradynamic tasks. Science Robotics 6 (2021). https://doi.org/10.1126/scirobotics.abf1628
19. Gross R, Tuci E, Dorigo M, Bonani M, Mondada F. Object transport by modular robots that self-assemble. Paper presented at 2006 IEEE International Conference on Robotics and Automation (ICRA), Orlando, FL, USA, 15-19 May, IEEE, pp. 2558-2564, 2006. https://doi.org/10.1109/ROBOT.2006.1642087
20. Yim M, Zhang Y, Duff D. Modular robots. IEEE Spectrum 39 (2002) 30-34.
21. Wolfe KC, Moses MS, Kutzer MD, Chirikjian GS. M 3 Express: a low-cost independently-mobile reconfigurable modular robot. Presented at 2012 IEEE International Conference on Robotics and Automation (ICRA), Saint Paul, MN, USA, 14-18 May, IEEE, pp. 2704-2710, 2012.
22. Yi S, Temel Z, Sycara K. PuzzleBots: physical coupling of robot swarms. Presented at 2021 IEEE International Conference on Robotics and Automation (ICRA), Xi'an, China, 30 May – 5 June, IEEE, pp. 8742-8748, 2021.
23. Knizhnik G, Yim M. Docking and Undocking a Modular Underactuated Oscillating Swimming Robot. Presented at 2021 IEEE International Conference on Robotics and Automation (ICRA), Xi'an, China, 30 May – 5 June, IEEE, pp. 6754-6760, 2021.
24. Siegwart R, Nourbakhsh IR, Scaramuzza D. Introduction to autonomous mobile robots, second ed. MIT press, 2011.